Chinese Chemical Letters 33 (2022) 115–122

Contents lists available at ScienceDirect

Chinese Chemical Letters

journal homepage: www.elsevier.com/locate/cclet

Near-infrared absorbing (>700 nm) aza-BODIPYs by freezing the rotation of the aryl groups

Yanyan Wang[a,1], Dongxiang Zhang[a,1], Kangming Xiong[b], Rong Shang[c], Xin-Dong Jiang[a,*]

[a] Shenyang Key Laboratory of Functional Dye and Pigment, Shenyang University of Chemical Technology, Shenyang 110142, China
[b] CAS Key Laboratory of Separation Science for Analytical Chemistry, Dalian Institute of Chemical Physics, Chinese Academy of Sciences, Dalian 116023, China
[c] Department of Chemistry, Graduate School of Science, Hiroshima University, Higashi-Hiroshima 7398526, Japan

ARTICLE INFO

Article history:
Received 21 April 2021
Revised 10 June 2021
Accepted 28 June 2021
Available online 5 July 2021

Keywords:
Aza-BODIPY
NIR
Ring-fused
Red shift
Freezing rotation

ABSTRACT

The typical aza-BODIPYs in the dye family are known for bright fluorescence, excellent stability, and tunable absorption wavelengths. Hence, these dyes are attracting the increasing attention. Aza-BODIPYs having the maxima absorption in the near-infrared (NIR) region (650–900 nm) are very favorable for bioimaging *in vivo* due to the less photo-damage, deeper tissue penetration, and less interference from background auto-fluorescence by biomolecules in the living systems. Many strategies have been employed to modify the structures of the aza-BODIPY core to provide the NIR absorbing dyes. Among these, the most effective method is the fusion of the aromatic rings in aza-BODIPY system. This review allsidedly summarizes the recent development of ring-fused aza-BODIPY dyes (λ_{abs} > 700 nm) focusing on the design, synthesis, and potential applications in the NIR region since 2002.

1. Introduction

Near-infrared (NIR) absorbing (λ_{abs} > 650 nm) dyes are found to have many especial applications. For example, fluorescence imaging techniques are widely used for visualizing and analyzing the localization of ions, cations and biomolecules [1]. However, excitation wavelengths (λ_{ex} < 650 nm) have low-grade tissue penetration, and therefore, are applicable for superficial structures or small animal imaging. Fluorophores requiring excitation at about 600 nm results in excessive autofluorescence because the bulk of naturally occurring endogenous fluorophores, mostly hemoglobin and related molecules, are also excited in the same region. Therefore, the optimal excitation wavelength (λ_{ex} > 650 nm) for a fluorophore is advocated, due to the combined virtues of deep tissue penetration, minimum photo-damage to biological samples, and low autofluorescence [2]. On the other hand, organic solar cells (OSCs) play an important role in the increase of the energy demand. However, one of the disadvantages of OSCs is the lack of light-harvesting in the NIR region beyond 700 nm, behaving 43% of the total energy flux [3].

Aza-borondipyrromethenes (aza-BODIPYs) in the dye family have long-wavelength absorption ($\lambda_{abs} \geq$ 650 nm), high molar extinction coefficient, high fluorescent quantum yield, and narrow absorption and emission peaks [4]. So, aza-BODIPY dyes can satisfy the essential requirements of an ideal NIR fluorophore. Therefore, aza-BODIPYs can be extensively applied to chemosensors [5,6], biological imaging [7–10], organic light-emitting [11], photosensitizers for photodynamic therapy [12–16] and other fluorescent functional dyes [17,18]. Compared to the traditional BODIPY dye, by the introduction of an imine replacing a methene in BODIPY system to effectively narrow the HOMO-LUMO gap one gives aza-BODIPY that are well-known to be an attractive dye to achieve the NIR absorption [19,20]. Importantly, π-π conjugated extension and freezing the rotation of the aryl groups in aza-BODIPY system are particularly promising and can effectively achieve the significant bathochromic-shift of absorption and emission bands into the NIR region [21,22]. For instance, photoacoustic (PA) dyes, absorbing the NIR light to provide ultrasonic signals, can be probed at centimeter depths in tissues by fluorescence-based methods [23,24]. Therefore, NIR absorbing (λ_{abs} > 700 nm) aza-BODIPYs have received widespread attention over the last decade [25].

Recently, our group summarized the three syntheticisms for aza-BODIPYs firstly (Scheme 1) [26]. Killoran *et al.* have explored novel routes to synthesize aza-BODIPYs by 1,3-diaryl-4-nitrobutan-one or 3-methyl-4-nitro-1-arylbutan-one (Scheme 1a), which can smoothly synthesize the symmetric/asymmetric construction of aza-BODIPYs widespreadly [27]. Aryl-fused aza-BODIPYs reported by Donyagina *et al.* were prepared in one-pot reaction by the

* Corresponding author.
E-mail address: xdjiang@syuct.edu.cn (X.-D. Jiang).
[1] These authors contributed equally to this work.

https://doi.org/10.1016/j.cclet.2021.06.083
1001-8417/

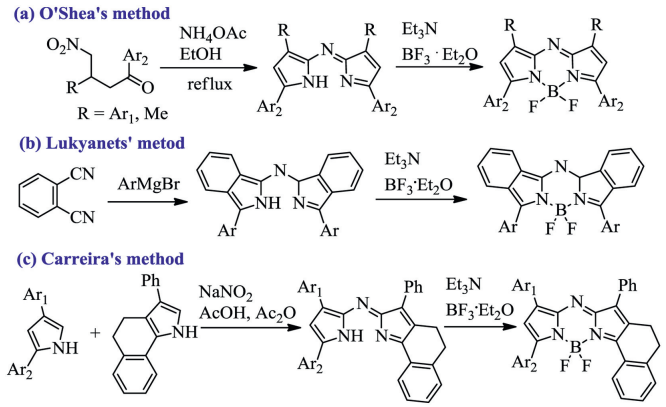

Scheme 1. Synthetic methods of the aza-BODIPYs.

reaction of an aryl magnesium bromide with a phthalonitrile (Scheme 1b) [28]. Utilizing 2,4-diaryl pyrrole or aryl-fused 2,4-diaryl pyrrole, Zhao and Carreira showed an efficient route of symmetric/asymmetric aza-BODIPYs (Scheme 1c) [29]. Compared to the product yields of O'Shea's and Lukyanets' methods, the product yield of Carreira's method is higher (beyond 40%). Moreover, compared to O'Shea's molecular structures, Lukyanets' and Carreira's molecular structures have larger conjugated surface of the parent molecules. In the past decade, our group focused on the design of aza-BODIPYs bearing the restricted rotation of the aryl groups in order to obtain NIR absorbing aza-BODIPYs. Very recently, Shi *et al.* reported a review paper from the perspective of rational structural design about bioapplications of micromolecule aza-BODIPYs derivated by O'Shea's method [30]. However, the design and synthesis of ring-fused aza-BODIPY dyes (λ_{abs} > 700 nm) were not systematically introduced in those review papers. By the strategy of freezing the free rotation of the aryl groups, we concluded design and synthesis of ring-fused aza-BODIPYs in this review. We also described the detailed spectral and photophysical data to provide the meaningful guidance for further design of NIR organic fluorescent materials.

Since the typical tetraphenyl-based aza-BODIPY **1** possessed a NIR absorption (λ_{abs} = 650 nm) and emission spectra, the strategies by restricting the rotation of the aryl groups could directly achieve a longer wavelength (λ_{abs} > 700 nm) for aza-BODIPYs (Scheme 2). Six kinds of synthetic strategies of the ring-fused aza-BODIPYs are shown in Schemes 2. For example, aza-BODIPY containing the phenyl-fused groups at 1,2/6,7-positions has a NIR absorbing spectra ($\lambda_{abs} \geq$ 710 nm) (aza-BODIPY **3c**) [28], and aza-BODIPY bearing the aryl-fused groups at 2,3/5,6-positions shows the maximum absorption beyond 700 nm (aza-BODIPY **18**) [29]. Moreover, the NIR fluorescent aza-BODIPY bearing all aryl-fused groups at 1,2,3/5,6,7-positions (aza-BODIPY **49**) [31], even possesses a NIR absorbing spectra at 882 nm. The details are as follows.

2. Ring-fused aza-BODIPYs

2.1. The upper aryl-fused aza-BODIPYs

Owing to the direct fusion of the upper aryl-group with the pyrrole of aza-BODIPY core to extend π-π conjugation (path *a*, Scheme 2), the upper aryl-fused aza-BODIPYs possess longer wavelength absorption in NIR region. In comparison with the typical dye aza-BODIPY **1**, the upper aryl-fused aza-BODIPYs were found to have an apparent advantage of the longer absorption wavelengths (Fig. 1 and Table 1) [32,33]. In 2011, Gresser *et al.* reported that the precursors **2a–f** and aza-BODIPYs **3a–f** were obtained by

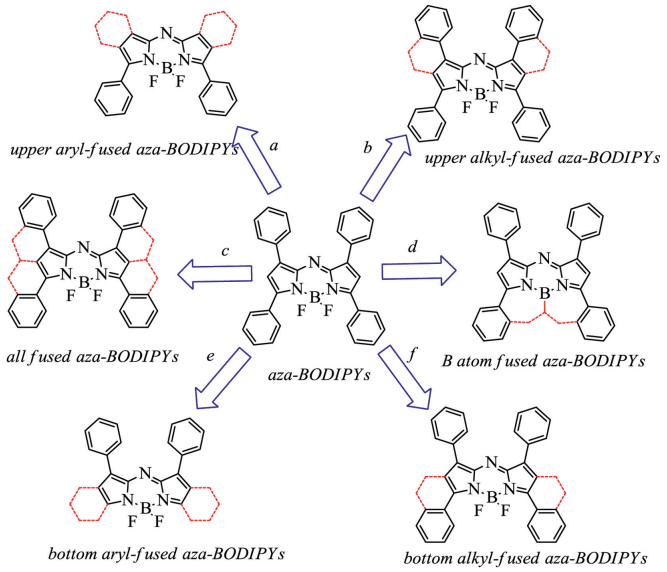

Scheme 2. Strategies for the NIR absorbing (λ_{abs} > 700 nm) aza-BODIPYs.

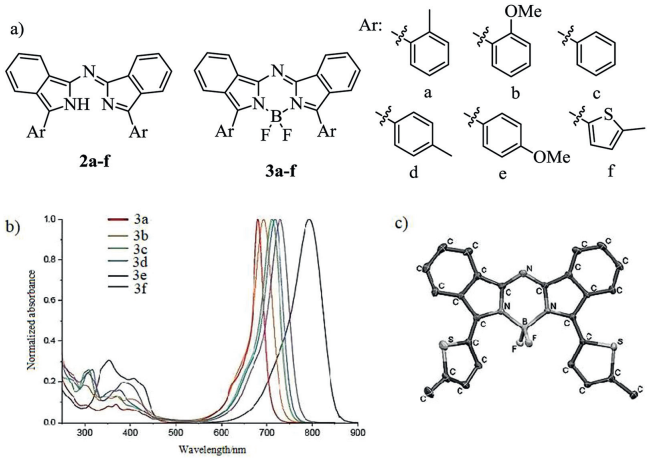

Fig. 1. Molecular structures, absorption spectra and single crystal. (a) Structures of dyes **2a–3f**. (b) Absorption spectra of **3a–f**. (c) X-ray analysis of **3f**. Reproduced with permission [34]. Copyright 2011, John Wiley and Sons.

reduce reaction and complex reaction with Grignard reagent and BF_3·OEt_2 (Fig. 1) [34]. The corresponding aza-BODIPYs **3** show a weak absorption in the visible region and the maxima absorption are bathochromic-shift into the NIR region beyond 790 nm, leading to a transparent window in the NIR region. Molecular orbital (MO) calculations clearly confirmed that the bathochromic-shift in aza-BODIPYs **3a–f** was caused by an increase of the HOMO levels. Based on the X-ray analysis of **3f**, the coplane of the aza-BODIPY core was confirmed.

Via the substitute of the fluorine atom in aza-BODIPY **3c** (Fig. 1), the functional aza-BODIPY derivatives **4** and **5** were developed to satisfy the practical applications of fluorescent dyes [32,34]. Due to a highly thermal stability, CN-substituted aza-BODIPYs can be successfully purified by vacuum sublimation. This upgrades thin film of high purity and quality, suggesting them suitable as candidates for vacuum-processed NIR organic electronic devices (Fig. 2b and Table 1).

In 2017, Li *et al.* extended the π-π conjugated structures by introducing the heterocyclic moieties and synthesized the NIR aza-BODIPYs *via* the heterocyclic organolithium reagents (Fig. 3 and Table 1) [33]. Then, aza-BODIPYs were further modified to re-

Table 1
Dyes and their optical properties.

Dye	$\lambda_{abs}/\lambda_{em}$ (nm)	ε (10^5 L mol^{-1} cm^{-1})	Stokes shift (nm)	Φ_f
2a	615/–	0.41	–	–
2b	640/–	0.47	–	–
2c	653/–	0.56	–	–
2d	657/–	0.55	–	–
2e	668/–	0.60	–	–
2f	720/–	0.40	–	–
3a	681/723	0.79	42	nf
3b	693/734	0.85	41	nf
3c	715/748	1.06	33	nf
3d	718/756	0.94	38	nf
3e	729/769	0.91	40	nf
3f	793/841	0.95	48	nf
4	722/754	0.9636	32	nf
5	717/752	0.9225	35	nf
6a	664/–	0.47	–	–
6b	762/798	0.70	36	0.37
6c	774/805	1.045	31	0.40
7a	689/–	0.445	–	–
7b	777/827	0.651	50	0.23
7c	793/840	0.686	47	0.26
8a	723/–	0.639	–	–
8b	793/840	0.896	47	0.09
8c	797/849	0.982	52	0.12

Spectral data are measured in dichloromethane. nf represents not found.

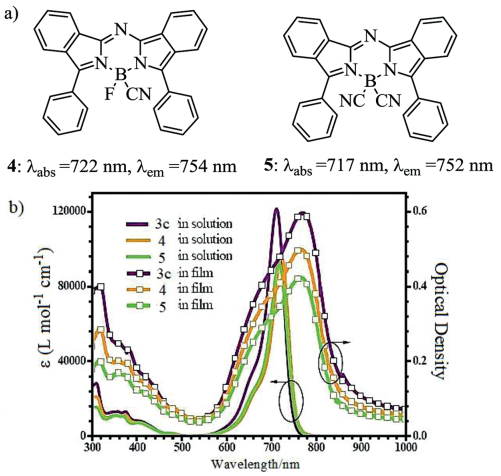

Fig. 2. Molecular structures and absorption spectra. (a) Aza-BODIPYs with bearing the –CN group. (b) Absorption spectra of **3c, 4** and **5** in CH_2Cl_2 solution and in film. Reproduced with permission [32]. Copyright 2017, John Wiley and Sons.

place one of the fluorine atoms with a cyanide which has the strong electron-withdrawing effect. As the NIR absorbing dyes, these dyes present high molar extinction coefficients (65,100–104,500 L mol^{-1} cm^{-1}) with absorption maxima in the NIR region between 762 and 797 nm. Based on the vacuum-deposited thin films, the absorption bands are red-shifted, peaking at 830–849 nm and broadened, giving the NIR donor materials for the vacuum-processed solar cells (Fig. 3b). Cyclic voltammetry (CV) measurements and MO calculations indicate that the HOMO-LUMO orbital levels are suited as donor materials in the solar cells while combined with the C_{60} compound as an acceptor.

In 2020, Diaz-Rodriguez *et al.* prepared Cl-aza-BODIPY **9** and pH-aza-BODIPY **10** (Fig. 4) [35]. Cl-aza-BODIPY scaffold **9** facilitates the substitutions at the boron atom to provide **10** by the treatment with phenyl Grignard reagent. pH-aza-BODIPY **10** was found to have a lower quantum yield, and this is mainly due to efficient non-radiative relaxation pathways offered by the free rotation of the numerous phenyl groups, particularly of the B-phenyl moieties. The maxima absorption of the pyrazine-fused aza-BODIPY **11**

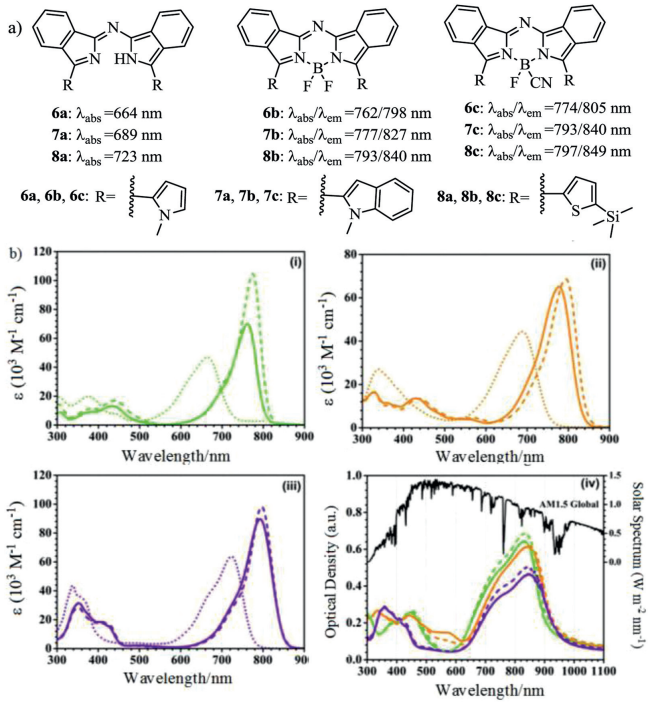

Fig. 3. Molecular structures and absorption spectra. (a) Structures of dyes **6–8**. (b) Absorption spectra of **6a–c** (i), **7a–c** (ii) and **8a–c** (iii) in CH_2Cl_2 (1×10^{-5} mol/L) and (iv) the absorption spectra in solid state as 50 nm thin film on glass. Reproduced with permission [33]. Copyright 2017, Royal Society of Chemistry.

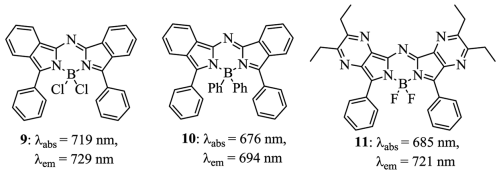

Fig. 4. Structures of aza-BODIPYs **9**–**11**.

Table 2
Dyes **9**–**14** and their optical properties.

Dye	$\lambda_{abs}/\lambda_{em}$ (nm)	ε (10^5 L mol^{-1} cm^{-1})	Stokes shift (nm)	Φ_f
9[a]	719/729	0.55	10	nf
10[a]	676/694	0.78	18	nf
11[b]	737/753	0.71	16	nf
12[c]	591/654	0.26	63	0.34
13[d]	728/739	nf	11	0.3
14[b]	673/774	0.5	101	0.005

nf represents not found.
[a] Represents testing in toluene.
[b] Represents testing in dichloromethane.
[c] Represents testing in THF.
[d] Represents testing in chloroform.

is 685 nm [36], which blue-shifts 24 nm, compared to that of **3c**. The hypochromatic-shift is mainly attributed to the higher electronegativity of the nitrogen atoms in pyrazine, which enhances the HOMO-LUMO band gap. Aza-BODIPY **11** can be applied for a colorimetric and fluorometric sensor for NH_4^+ (Fig. 4 and Table 2).

In 2017, Zheng *et al.* showed the novel aza-BODIPY **12** from phthalonitrile in *t*-BuOK solution in a facile manner on large scale (Fig. 5) [37–39]. The asymmetric aza-BODIPY **12** prompts the weak B-N bond breakage in the presence of TFA, giving a sharp color change from red to colorless (Fig. 5c and Table 2).

The introduction of 1,2-naphtho-fused rings to produce dye **13** leads to a 25 nm bathochromic-shift of the maxima absorption rel-

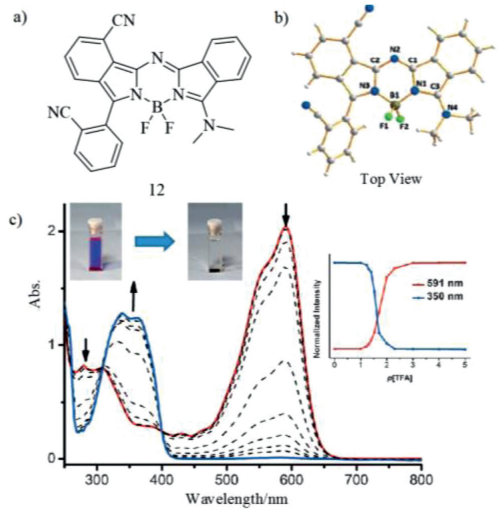

Fig. 5. Molecular structures, single crystal and absorption change. (a) Benzo-fused aza-BODIPY **12** and (b) X-ray analysis of dye **12**. (c) Absorption spectra of aza-BODIPY **12** with TFA. Reproduced with permission [37]. Copyright 2015, John Wiley and Sons.

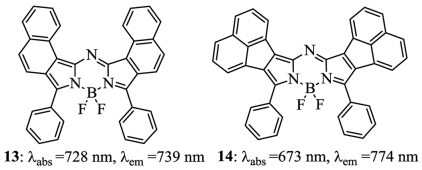

Fig. 6. Structures of aza-BODIPYs **13** and **14**.

Table 3
Dyes **15**–**17** and their optical properties.

Compound	$\lambda_{abs}/\lambda_{em}$ (nm)	ε (10^5 L mol^{-1} cm^{-1})	stokes shift (nm)	Φ_f
15a[a]	745/771	1.247	26	0.35
15b[a]	716/741	1.477	25	0.32
16[b]	757/803	0.795	46	0.047
17[c]	688/725	0.255	37	0.26

[a] Spectral data are measured in toluene.
[b] Represents testing in chloroform.
[c] Represents testing in dichloromethane.

ative to that of the parent dye **3c** (Fig. 6 and Table 2), along with a slight change in other optical properties [40,41]. Majumdar *et al.* reported a NIR absorbing acenaphthalene-fused aza-BODIPY dye **14**, which broad absorption band at the red terminal of the visible region, providing possibilities for the application in the field of solar cells [42].

2.2. The upper alkyl-fused aza-BODIPYs

By the interlinkage of the σ single bond (path *b*, Scheme 2), a new substitution pattern of aza-BODIPYs were synthesized by the upper phenanthrene fusion by a key Pd-catalyzed intramolecular C–H activation reaction (Figs. 7a and b) [31]. Such phenanthrene-fused aza-BODIPYs have strong red-shifted NIR absorptions and high fluorescent quantum yields (Table 3). Aza-BODIPY **15a** has a planar structure of the phenanthrene-fused aza-BODIPY core by X-ray analysis (Fig. 7c). Aza-BODIPY **15a** having low cytotoxicity, can stain the HepG2 cells, indicating a bright NIR bioimaging nature (Fig. 7d and Table 3).

Zhou *et al.* reported a restricted aza-BODIPY **16** for the NO probe with enhanced photoacoustic properties (Fig. 8), by utilizing the upper phenyl-fused pyrrole with the -CH_2-CH_2- alkyl chain for the first time (path *b*, Scheme 2) [43]. Compared to **3c**, aza-

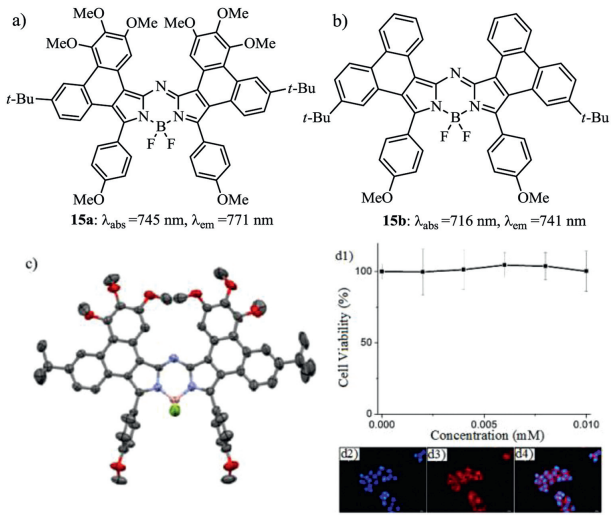

Fig. 7. Structures of (a) aza-BODIPY **15a** and (b) aza-BODIPY **15b**. (c) X-ray analysis of **15a**. (d1) Fluorescence images of HepG2 cells stained with **15a** (5.0 μmol/L) and DAPI (1.67 μg/mL), d2) DAPI fluorescence, (d3) **15a** fluorescence, and (d4) merged images of parts d2 and d3. Reproduced with permission [31]. Copyright 2017, American Chemical Society.

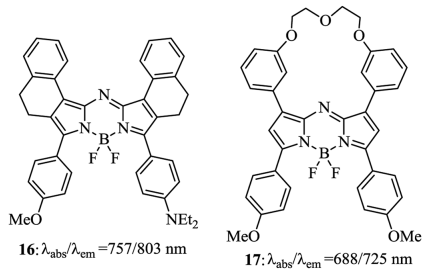

Fig. 8. Structures of the upper phenyl-restricted aza-BODIPY **16** and **17**.

BODIPY **16** formed by connecting the 1,7-positions of the phenyl groups with the 2,6-positions of aza-BODIPY by the alkyl chain can further improve the spectral properties. To restrict the free rotation of the phenyl group in 1,7-positions similar to the molecule **16**, aza-BODIPY **17** with two phenyl groups linked by oligoethylene glycol chains was synthesized and applied for intracellular imaging for HepG2 cells (Fig. 8 and Table 3) [44].

2.3. The bottom alkyl-fused aza-BODIPYs

Zhao and Carreira reported the novel NIR conformational restricted aza-BODIPYs **18–29** (Fig. 9) prepared by an efficient process in 2006 for the first time (path *c*, Scheme 2) [29,45]. By tunable substitution and restriction, the bottom alkyl-fused aza-BODIPY dyes have the long-wavelengh fluorescence at 700–900 nm, high fluorescence quantum yield, narrow full width at half maximum and remarkable photostability (Table 4) [46–51]. The morpholine-containing aza-BODIPY **29** as a probe can detect the pH value. Additionally, aza-BODIPY with the sulfur atom **21** as a photosensitizer (PS) could generate the single oxygen.

In 2018, Jiang *et al.* prepared five-membered-ring fused aza-BODIPY **30** (Fig. 10) [52]. Such aza-BODIPY has long absorption/emission wavelength, high molar extinction coefficient, and narrow excitation/emission peak. However, the planar structure of **30** could not obviously enhance the optical properties than these of six-membered-ring fused aza-BODIPY. In 2015, Jiang *et al.* reported the symmetric pyrene-containing aza-BODIPY **31** in the NIR region (λ_{abs} = 746 nm, λ_{em} = 762 nm), based on the combined

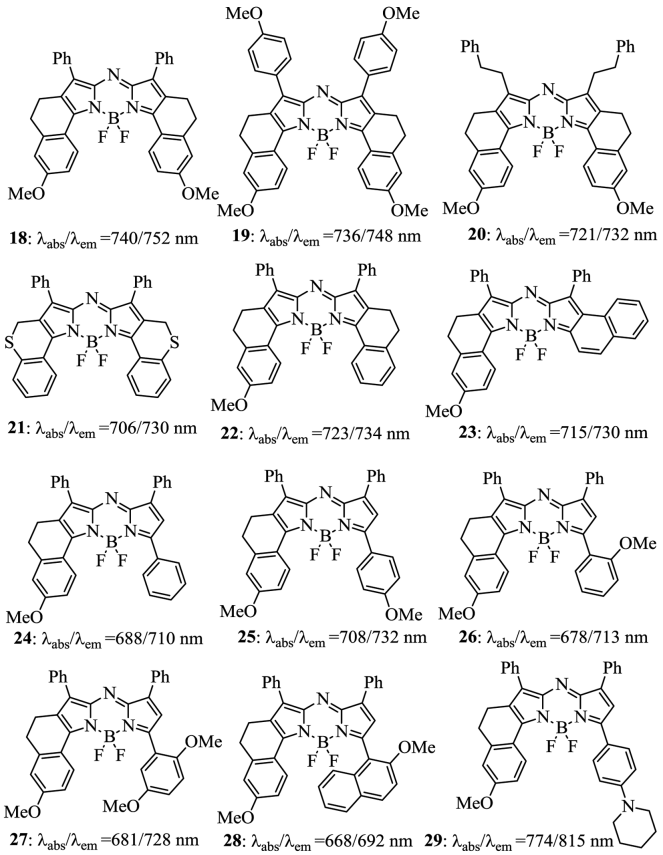

Fig. 9. Structures of aza-BODIPY dyes **18–29**.

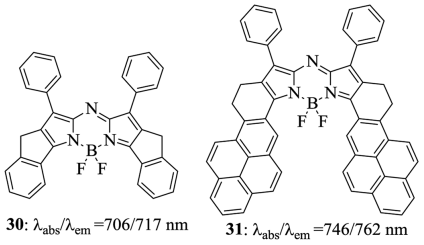

Fig. 10. Five-membered-ring fused aza-BODIPY **30** and pyrene-containing aza-BODIPY **31**.

Table 4
Dyes **18–40** and their optical properties.

Compound	$\lambda_{abs}/\lambda_{em}$ (nm)	ε (10^5 L mol^{-1} cm^{-1})	stokes shift (nm)	Φ_f
18	740/752	1.59	12	0.28
19	736/748	1.57	12	0.29
20	721/732	1.62	11	0.31
21	706/730	1.15	24	0.11
22	723/734	1.57	11	0.32
23	715/730	1.41	15	0.11
24	688/710	1.08	22	0.44
25	708/732	0.962	24	0.38
26	678/713	0.839	35	0.38
27	681/728	0.665	47	0.24
28	668/692	1.13	24	0.46
29	774/815	0.703	41	0.05
30	706/717	1.29	11	0.34
31	746/762	1.48	16	0.16
32	717/734	0.48	17	0.03
33	735/755	0.63	20	0.14
34[a]	760/782	1.36	22	0.19
35a	731/749	1.66	18	0.18
35b	746/780	1.53	34	0.12
36[a]	796/813	1.72	17	0.12
37[a]	759/791	1.57	32	0.19
38[a]	789/822	1.35	33	0.04
39[a]	759/785	0.905	26	0.19
40[a]	782/818	0.892	36	0.06

Spectral data are measured in dichloromethane.
[a] Spectral data are measured in chloroform.

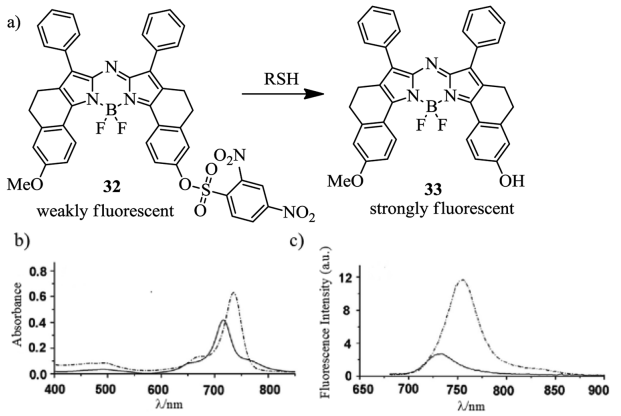

Fig. 11. Reaction mechanism and spectral variation. (a) Reaction of aza-BODIPY with RSH. (b) Absorption and (c) Emission spectra (λ_{ex} = 670 nm) of probe **32** before (solid curve) and after (dashed curve) the addition of cysteine. Reproduced with permission [54]. Copyright 2012, Royal Society of Chemistry.

effect of the extension of the π-π conjugation and the rigidization (Fig. 10) [53]. Restricting the free rotation and extending the conjugation by introducing the pyrenyl substituent in **31** effectively promote bathochromic-shift (110 nm), comparing to that of **1**. The decrease in the HOMO-LUMO band gap for the lowest energy absorption bands was observed in the pyrene-fused aza-BODIPY (Table 4).

In 2012, Jiang *et al.* synthesized a turn-on aza-BODIPY-based NIR fluorescent probe **32** (Fig. 11) [54]. The maxima absorption and emission of probe **32** were 717 nm (ε = 48,000 L mol^{-1} cm^{-1}) and 734 nm, respectively. Dye **32** displayed weakly fluorescent (Φ_f = 0.03) (the solid curve in Fig. 11c). When adding cysteine, the maxima absorption and emission wavelengths were bathochromic-shifted to 735 nm and 755 nm, respectively, and markable enhanced quantum yield (Φ_f = 0.14) was achieved (Fig. 11 and Table 4).

In 2016, Jiang *et al.* reported aza-BODIPY **34** containing the thiophene groups (Fig. 12a) [55]. Aza-BODIPY **34** has absorption/emission wavelengths of 760/782 nm in the NIR region. Aza-BODIPY **34** as a typical NIR chemical sensor is highly selective to Hg^{2+}. The mechanism of fluorescence quenching is the transfer of electrons from thiophene groups to the aza-BODIPY core by binding to Hg^{2+} (Fig. 12b and Table 4).

In 2014, the styryl-containing asymmetric aza-BODIPYs **35** by Jiang *et al.* were prepared in the NIR region for the first time, which was bright enough for labeling the living cells for fluorescence imaging assays (Fig. 13 and Table 4) [56]. In short, the asymmetric aza-BODIPYs enrich the quantities and categories of aza-BODIPYs which can be used to meet the purpose of the application. Compared to symmetrical aza-BODIPYs, asymmetric aza-BODIPYs are not easily synthesized, with lower yield.

In 2019, Zhou *et al.* developed aza-BODIPYs with the -CH_2–CH_2- alkyl chain and investigated their absorbance, fluorescence, and photoacoustic (PA) properties (Fig. 14) [43,57]. All conformationally restricted aza-BODIPYs **36–40** had the promotion in the molar absorptivity owing to the increased complanarity between the aza-BODIPY core and the aryl groups. MO studies indicated that the aryl groups at 3,5-positions in aza-BODIPY system efficiently

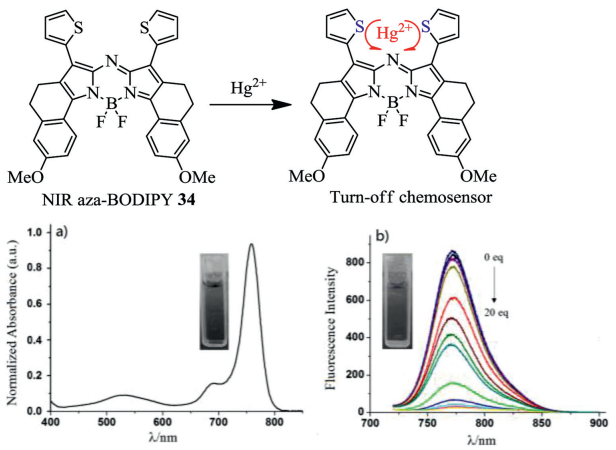

Fig. 12. Spectral changes of (a) absorption spectrum of NIR fluorescent probe **34** with Hg^{2+}. (b) Emission spectra of NIR fluorescent probe **34** with Hg^{2+}. Reproduced with permission [55]. Copyright 2015, Elsevier.

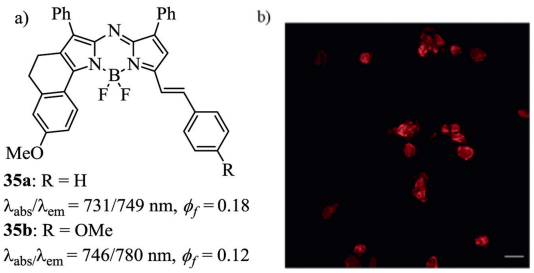

Fig. 13. Molecular structures and cell staining. (a) Styryl-containing aza-BODIPYs **35**. (b) Image of living cells stained by dye **35b**. Reproduced with permission [56]. Copyright 2014, Royal Society of Chemistry.

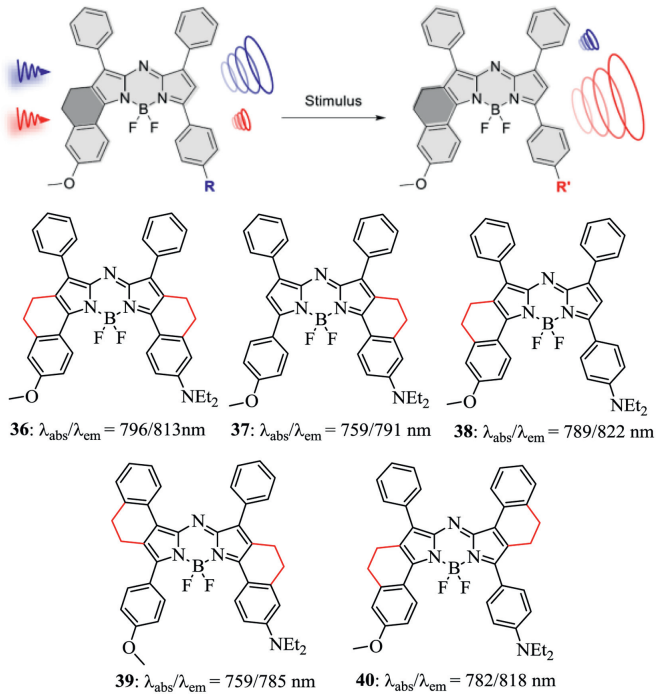

Fig. 14. Restricted-aryl aza-BODIPY dyes **36–40**. Reproduced with permission [43]. Copyright 2019, American Chemical Society.

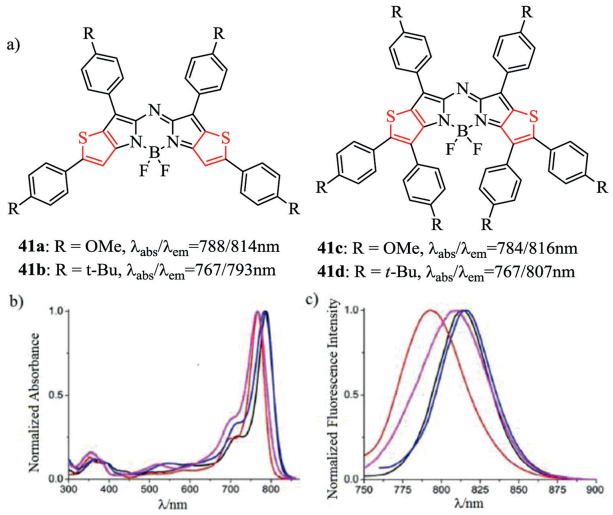

Fig. 15. Molecular structures and optical spectra. (a) Thiophenyl-fused aza-BODIPYs **41**. (b) Normalized UV−vis and (c) fluorescence spectra of aza-BODIPYs **41a** (black), **41b** (red), **41c** (blue), **41d** (magenta) in chloroform. Reproduced with permission [58]. Copyright 2014, American Chemical Society (For interpretation of the references to color in this figure legend, the reader is referred to the web version of this article.).

Table 5
Dyes **41a–41d** and their optical properties.

Compound	$\lambda_{max,abs}$ (nm)	ε (10^5 L mol^{-1} cm^{-1})	stokes shift (nm)	Φ_f
41a	788/814	1.7	26	0.10
41b	767/793	2.239	26	0.12
41c	784/816	1.82	32	0.04
41d	767/807	1.445	40	0.05

Spectral data are measured in chloroform.

enhance the HOMO levels than those at 1,7-positions (Fig. 14). It was found that the free rotation of the aryl-groups was important to maximizing $\Delta\lambda$, while restriction of the aryl-groups was found to enhance the PA signal by increasing the extinction coefficient without promoting quantum yield markedly (Table 4).

2.4. The bottom aryl-fused aza-BODIPYs

To the direct fusion of the bottom aryl-group in 2,3/5,6-posions in aza-BODIPY system, in 2014 Kamkaew *et al.* reported a series of the bottom thiophenyl-fused aza-BODIPYs **41** (path *d*, Scheme 2) [44,58]. Aza-BODIPYs **41** with the stronger and sharper absorption above 800 nm, absorbing weaker in the visible spectrum region from 380 nm to 700 nm were obviously observed (Fig. 15 and Table 5). The excellent optical properties and simple synthesis of aza-BODIPYs **41** have led to further application in biotechnology and material science.

2.5. B atom-fused aza-BODIPYs

Linking the ortho-positions of the phenyl groups to the central atom B can establish aza-BODIPYs **43** and **44** with the six-member heterocyclic ring (path *e*, Scheme 2, Fig. 16) [59,60]. Comparing to aza-BODIPY **42**, the restricted dye **43** displays obviously absorption and emission bathochromic-shift of up to 86/58 nm (Table 6). The favorable emission wavelength and fluorescent quantum yield are strongly indicative of the future applications in biotechnology.

To excavate the steric hindrance effect similar to aza-BODIPYs **42–43** with the six-member heterocyclic ring, in 2016 Jiang *et al.* reported aza-BODIPY dyes bearing 1-methyl-1*H*-pyrrolyl groups at 3,5-positions (Fig. 17 and Table 6) [61]. Aza-BODIPY **45** absorbs at 721 nm and emits at 751 nm, respectively. However, aza-BODIPY **46** has long wavelengths of absorption and emission

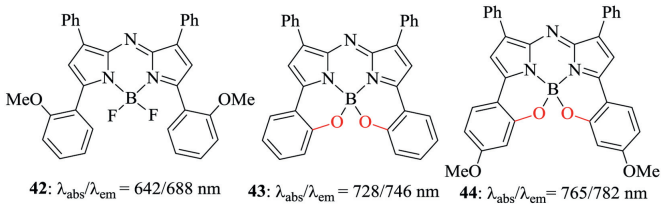

Fig. 16. B,O–chelated aza-BODIPYs.

Table 6
Dyes **42**–**46** and their optical properties.

Compound	$\lambda_{max,abs}$ (nm)	ε (10^5 L mol^{-1} cm^{-1})	stokes shift (nm)	Φ_f
42	642/688	nf	46	0.07
43	728/746	nf	18	0.51
44	765/782	nf	17	0.18
45[a]	721/751	1.15	30	0.37
46[a]	754/803	1.1	49	0.26

Spectral data are measured in chloroform. nf represents not found.
[a] Spectral data are measured in dichloromethane.

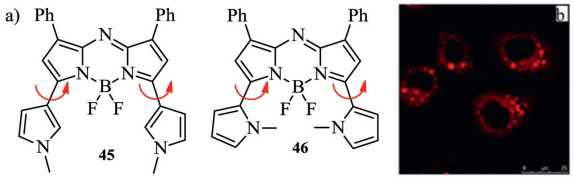

Fig. 17. Molecular structures and cell staining. (a) Methylpyrrolyl-containing aza-BODIPYs. (b) Image of living cells stained by dye **46**. Reproduced with permission [61]. Copyright 2016, John Wiley and Sons.

Table 7
Dyes **47**–**49** and their optical properties.

Compound	$\lambda_{max,abs}$ (nm)	ε (10^5 L mol^{-1} cm^{-1})	stokes shift (nm)	Φ_f
47	826/832	4.494	6	0.07
48	850/873	2.354	23	<0.01
49	878/907	2.601	29	0.13

Spectral data are measured in toluene.

(λ_{abs} = 754 nm, λ_{em} = 803 nm) than these of the corresponding aza-BODIPY **45**. Comparing to aza-BODIPY **45**, the rotation of the pyrrolic group in **46** is be slowed or prohibited, due to the steric hindrance between the pyrrolic group and the fluorine atom at the boron center. These reveal the favourable consistency with the discrepant optical contrast between the restricted aza-BODIPY caused by the B-O bonds and its precursor by Burgess and O'Shea *et al.* Aza-BODIPY **45** could stand pH 12 and is more stable than dye **1**, and was suitable for labeling the living cells for fluorescence imaging assay in the NIR region.

2.6. All ring-fused aza-BODIPYs

In 2018, Sheng *et al.* synthesized NIR fluorescent aza-BODIPYs **47, 48** and **49** containing the aryl-fused group at 1,2,3/5,6,7-positions using $FeCl_3$ (path *f*, Scheme 2, Fig. 18a) [62]. These aza-BODIPYs have unique structures (Fig. 18b) and excellent optical properties with the NIR absorption and emission, high extinction coefficient up to 4.5 × 10^5 L mol^{-1} cm^{-1} and good photostability (Table 7). These dyes reveal their potential applications in the construction of organic fluorescent clusters based on annular fused nitrogen-hetero-specific groups for the first time. Theoretically, all aryl-fused structures have the longest absorption maxima, however the complex molecular design and difficult synthesis limit their application. Therefore, for all ring-fused aza-BODIPYs, more convenient synthesis method and extensive applications are forward to be explored.

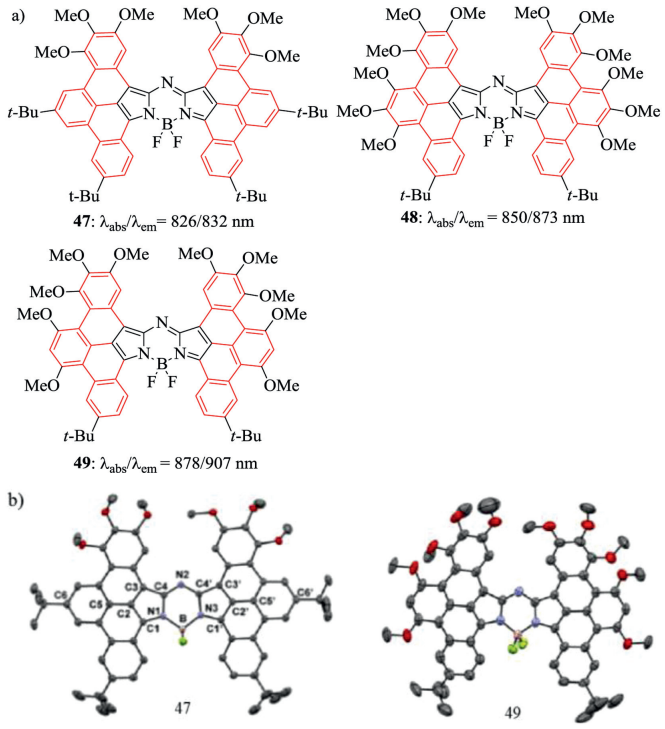

Fig. 18. Molecular structures and single crystal. (a) Aza-BODIPYs **47, 48** and **49**. (b) X-ray crystal structures **47** and **49**. Reproduced with permission [62]. Copyright 2018, American Chemical Society.

3. Summary

Compared with the classical aza-BODIPY **1** (λ_{abs} = 650 nm), ring-fused aza-BODIPYs (Scheme 2) possess higher molar absorption coefficient, longer wavelength of absorption spectra (λ_{abs} > 700 nm) in the NIR region. Aza-BODIPYs with the aryl-fused groups at 1,2/6,7-positions or 2,3/5,6-positions, aza-BODIPYs bearing the -CH_2- link to the aryl group at the upper or bottom position, and B-fused aza-BODIPYs with the six-member heterocyclic ring at 4-position have the NIR absorbing spectra between 700 and 800 nm. Moreover, aza-BODIPYs bearing all ring-fused groups at 1,2,3/5,6,7-positions even possess an absorption maxima beyond 800 nm. The ring-fused aza-BODIPYs presented in this review are expected to give a useful guidance for further developing the efficient NIR organic fluorophores with suitable properties for biomedical and material applications and so forth.

Declaration of competing interest

The authors declare that they have no known competing financial interests or personal relationships that could have appeared to influence the work reported in this paper.

Acknowledgments

This work was supported by the National Natural Science Foundation of China (Nos. 22078201, U1908202), "Chunhui Program" cooperative research project of Education Ministry, Liaoning BaiQianWan Talents Program, Serving local project of Education Department of Liaoning Province (No. LZ2020005) and the Distinguished Professor Project Liaoning Province (No. 20183532).

References

[1] M.A.T. Rogers, Nature 151 (1943) 504.
[2] A. Loudet, K. Burgess, Chem. Rev. 107 (2007) 4891–4932.
[3] R.S. Rao, B. Yadagiri, G.D. Sharma, S.P. Singh, Chem. Commun. 55 (2019) 12535–12538.
[4] M.A.T. Rogers, J. Chem. Soc. (1943) 590–596.
[5] P. Lu, X. Zhang, T. Ren, L. Yuan, Chin. Chem. Lett. 31 (2020) 2980–2984.
[6] M. Liu, S. Ma, M. She, Chin. Chem. Lett. 30 (2019) 1815–1824.
[7] S. Kolemen, E.U. Akkaya, Coord. Chem. Rev. 354 (2018) 121–134.
[8] W. Sheng, F. Lv, B. Tang, E. Hao, L. Jiao, Chin. Chem. Lett. 30 (2019) 1825–1833.
[9] L.L. Wang, W. Du, Z.J. Hu, Angew. Chem. Int. Ed. 58 (2019) 14026–14043.
[10] J. Weber, P.C. Beard, S.E. Bohndiek, Nat. Methods 13 (2016) 639–650.
[11] M. Chapran, E. Angioni, N.J. Findlay, ACS Appl. Mater. Interfaces 9 (2017) 4750–4757.
[12] Y. Yan, X. Zhang, X. Zhang, Chin. Chem. Lett. 31 (2020) 1091–1094.
[13] N. Boens, B. Verbelen, M.J. Ortiz, L. Jiao, W. Dehaen, Coord. Chem. Rev. 399 (2019) 213024.
[14] C. Wang, Q.L. Qiao, W.J. Chi, Angew. Chem. Int. Ed. 59 (2020) 10160–10172.
[15] J. Wang, Q.B. Gong, L. Wang, E. Hao, L.J. Jiao, J. Porphyr. Phthalocyanines 24 (2020) 603–635.
[16] J.J. Du, N. Xu, J.L. Fan, W. Sun, X.J. Peng, Small 15 (2019) 1805087.
[17] F. Deng, L.M. Liu, Q.L. Qiao, Chem. Commun. 55 (2019) 15045–15048.
[18] W.J. Chi, Q.L. Qiao, R. Lee, Angew. Chem. Int. Ed. 58 (2019) 7073–7077.
[19] N. Zhou, F. Huo, Y. Yue, K. Ma, C. Yin, Chin. Chem. Lett. 31 (2020) 2970–2974.
[20] W.L. Mao, M.M. Zhu, C.X. Yan, ACS Appl. Bio Mater. 3 (2020) 45–52.
[21] H. Lu, S. Shimizu, J. Mack, Z. Shen, N. Kobayashi, Chem. Asian J. 6 (2011) 1026–1037.
[22] H. Zhang, P. Xu, X. Zhang, Chin. Chem. Lett. 31 (2020) 1083–1086.
[23] H.J. Knox, J. Chan, Acc. Chem. Res. 51 (2018) 2897–2905.
[24] J. Weber, P.C. Beard, S.E. Bohndiek, Nat. Methods 13 (2016) 639–650.
[25] A. Mishra, P. Baüerle, Angew. Chem. Int. Ed. 51 (2012) 2020–2067.
[26] X.D. Jiang, S. Li, J. Guan, Curr. Org. Chem. 20 (2016) 1736–1744.
[27] J. Killoran, L. Allen, J.F. Gallagher, W.M. Gallagher, D.F. O'Shea, Chem. Commun. (2002) 1862–1863.
[28] V.F. Donyagina, S. Shimizu, N. Kobayashi, E.A. Lukyanets, Tetrahedron Lett. 49 (2008) 6152–6154.
[29] W. Zhao, E.M. Carreira, Chem. Eur. J. 12 (2006) 7254–7263.
[30] Z.X. Shi, X. Han, W.B. Hu, Chem. Soc. Rev. 49 (2020) 7533–7567.
[31] W.L. Sheng, J.E. Cui, Z. Ruan, J. Org. Chem. 82 (2017) 10341–10349.
[32] T.Y. Li, Z.F. Ma, Z. Qiao, Chempluschem 82 (2017) 190–194.
[33] T.Y. Li, T. Meyer, R. Meerheim, J. Mater. Chem. A 5 (2017) 10696–10703.
[34] R. Gresser, M. Hummert, H. Hartmann, K. Leo, M. Riede, Chem. Eur. J. 17 (2011) 2939–2947.
[35] R.M. Diaz-Rodriguez, L. Burke, K.N. Robertson, A. Thompson, Org. Biomol. Chem. 18 (2020) 2139–2147.
[36] H.Z. Liu, J. Mack, Q.L. Guo, Chem. Commun. 47 (2011) 12092–12094.
[37] W. Zheng, B.B. Wang, C.H. Li, Angew. Chem. Int. Ed. 54 (2015) 9070–9074.
[38] K. Skonieczny, D.T. Gryko, J. Org. Chem. 80 (2015) 5753–5763.
[39] Y. Ni, W.D. Zeng, K.W. Huang, J.S. Wu, Chem. Commun. 49 (2013) 1217–1219.
[40] R. Berraud-Pache, F. Neese, G. Bistoni, R. Izsak, J. Phys. Chem. Lett. 10 (2019) 4822–4828.
[41] H. Lu, S. Shimizu, J. Mack, Z. Shen, N. Kobayashi, Chem. Asian J. 6 (2011) 1026–1037.
[42] P. Majumdar, J. Mack, T. Nyokong, RSC Adv. 5 (2015) 78253–78258.
[43] E.Y. Zhou, H.J. Knox, C. Liu, W.L. Zhao, J. Chan, J. Am. Chem. Soc. 141 (2019) 17601–17609.
[44] A. Kamkaew, S. Thavornpradit, T. Puangsamlee, Org. Biomol. Chem. 13 (2015) 8271–8276.
[45] W.L. Zhao, E.M. Carreira, Angew. Chem. Int. Ed. 44 (2005) 1677–1679.
[46] A. Burghart, H. Kim, M.B. Welch, J. Org. Chem. 64 (1999) 7813–7819.
[47] H. Kim, A. Burghart, M.B. Welch, J. Reibenspies, K. Burgess, Chem. Commun. (1999) 1889–1890.
[48] J. Chen, J. Reibenspies, A. Derecskei-Kovacs, K. Burgess, Chem. Commun. (1999) 2501–2502.
[49] J. Chen, A. Burghart, A. Derecskei-Kovacs, K. Burgess, J. Org. Chem. 65 (2000) 2900–2906.
[50] A. Gorman, J. Killoran, C. O'Shea, J. Am. Chem. Soc. 126 (2004) 10619–10631.
[51] M. Grossi, M. Morgunova, S. Cheung, Nat. Commun. 7 (2016) 10855.
[52] X.D. Jiang, X. Liu, T. Fang, C.L. Sun, L.J. Xiao, Tetrahedron Lett. 59 (2018) 546–549.
[53] X.D. Jiang, D.M. Xi, C.L. Sun, Tetrahedron Lett. 56 (2015) 4868–4870.
[54] X.D. Jiang, J. Zhang, X.M. Shao, W.L. Zhao, Org. Biomol. Chem. 10 (2012) 1966–1968.
[55] X.D. Jiang, J.L. Zhao, Q. Li, Dyes Pigments 125 (2016) 136–141.
[56] X.D. Jiang, D.M. Xi, J.L. Zhao, RSC Adv. 4 (2014) 60970–60973.
[57] H.J. Knox, J. Chan, Acc. Chem. Res. 51 (2018) 2897–2905.
[58] Y.Y. Wu, C. Cheng, L.J. Jiao, Org. Lett. 16 (2014) 748–751.
[59] Y. Ge, D.F. O'Shea, Chem. Soc. Rev. 45 (2016) 3846–3864.
[60] A. Loudet, R. Bandichhor, K. Burgess, Org. Lett. 10 (2008) 4771–4774.
[61] X.D. Jiang, J. Guan, Q. Li, C.L. Sun, Asian J. Org. Chem. 5 (2016) 1063–1067.
[62] W.L. Sheng, Y.Y. Wu, C.J. Yu, Org. Lett. 20 (2018) 2620–2623.